Relation between Heterogeneous Frozen Regions in Supercooled Liquids and Non-Debye Spectrum in the Corresponding Glasses

Matteo Paoluzzi,[1,*] Luca Angelani,[1,2] Giorgio Parisi,[1,3,4] and Giancarlo Ruocco[1,5]
[1]Dipartimento di Fisica, Sapienza Università di Roma, Piazzale A. Moro 2, I-00185, Rome, Italy
[2]ISC-CNR, Institute for Complex Systems, Piazzale A. Moro 2, I-00185 Rome, Italy
[3]Nanotec-CNR, UOS Rome, Sapienza Università di Roma, Piazzale A. Moro 2, I-00185, Rome, Italy
[4]INFN-Sezione di Roma 1, Piazzale A. Moro 2, I-00185, Rome
[5]Center for Life Nano Science, Istituto Italiano di Tecnologia, Viale Regina Elena 291, I-00161, Rome, Italy

(Received 29 January 2019; revised manuscript received 4 September 2019; published 11 October 2019)

Recent numerical studies on glassy systems provide evidence for a population of non-Goldstone modes (NGMs) in the low-frequency spectrum of the vibrational density of states $D(\omega)$. Similarly to Goldstone modes (GMs), i.e., phonons in solids, NGMs are soft low-energy excitations. However, differently from GMs, NGMs are localized excitations. Here we first show that the parental temperature T^* modifies the GM/NGM ratio in $D(\omega)$. In particular, the phonon attenuation is reflected in a parental temperature dependency of the exponent $s(T^*)$ in the low-frequency power law $D(\omega) \sim \omega^{s(T^*)}$, with $2 \leq s(T^*) \leq 4$. Second, by comparing $s(T^*)$ with $s(p)$, i.e., the same quantity obtained by pinning a p particle fraction, we suggest that $s(T^*)$ reflects the presence of dynamical heterogeneous regions of size $\xi^3 \propto p$. Finally, we provide an estimate of ξ as a function of T^*, finding a mild power law divergence, $\xi \sim (T^* - T_d)^{-\alpha/3}$, with T_d the dynamical crossover temperature and α falling in the range $\alpha \in [0.8, 1.0]$.

DOI: 10.1103/PhysRevLett.123.155502

Introduction.—At small enough frequencies ω, the density of states $D(\omega)$ of a three dimensional glass follows Debye's law $D(\omega) \sim \omega^2$. This is because at large enough length scale glasses are continuum media and thus phonons dominate the low frequency spectrum [1]. However, compared with crystals, glasses show thermodynamic anomalies at low temperatures. For instance, the thermal conductivity $\kappa(T)$ scales with T^2 [2] instead of T^3, as predicted by Debye's law [1]. Moreover, also the specific heat C_v below 1 K deviates from Debye's law acquiring a linear dependency on T [2]. Remarkably, these anomalies are shared by a broad class of glassy systems providing evidences of universality.

As it has been noticed in Ref. [3], in disordered media and small ω, $D(\omega)$ takes contributions from both extended Goldstone bosons, e.g., phonons in structural glasses or spin waves in Heisenberg spin glasses, and non-Goldstone modes, i.e., excitations that are not generated by the spontaneous symmetry breaking of a continuous symmetry. The Goldstone contribution gives rise to the Debye spectrum $D(\omega) \sim \omega^{d-1}$, with d the number of spatial dimensions. The non-Goldstone sector is still soft, i.e., normal modes whose density of states vanishes as a power law $D(\omega) \sim \omega^s$ [3], but it is populated by localized modes. Only in the last few years, thanks to the possibility of eliminating Goldstone bosons from the low-energy spectrum [4,5] or discriminating nonextended modes from the extended ones [6], it has been possible to observe numerically the non-Goldstone sector in numerical simulations obtaining that, in agreement with arguments suggested in Ref. [3], non-Goldstone modes give a contribution to $D(\omega)$ that scales with $s = 4$.

In a previous work, we showed that a population of soft-localized modes with $D(\omega) \sim \omega^{s(p)}$ and $2 \leq s(p) \leq 4$ emerges in the low-frequency spectrum of a three-dimensional model of glass when a fraction p of particles are randomly frozen [7]. In particular, the value of the effective exponent $s(p)$ starts from $s = 2$ at $p = 0$ and approaches 4 above a threshold p_{th} value that is of the order of 50% of frozen particles.

In this Letter we study the properties of the vibrational density of states of a model of glass in its inherent states, i.e., configurations that minimize the potential energy at $T = 0$. Inherent states have been obtained after a fast quench from equilibrium configurations at the parental temperature T^*. In agreement with Ref. [8], the slope in the tail of $D(\omega)$ depends on the parental temperature T^*. Moreover, as a first result, we observe a progressive attenuation of the Debye spectrum in favor of the non-Debye one as T^* approaches from above the dynamical crossover temperature T_d.

It turns out that the Debye scaling $s = 2$ holds at $T^* \gg T_d$, s increases by decreasing T^*, and it saturates to $s = 4$ right above T_d. This crossover between Debye to non-Debye is accompanied by a progressive localization of the normal modes below the boson peak. We will show that it is possible to relate the suppression of extended excitations with the proliferation of spatially heterogeneous regions. We observe that the behavior of $s(T^*)$ mirrors that

of $s(p)$ observed in Ref. [7], indicating an increase in the size of frozen heterogeneous regions as T^* decreases. This finding suggests a way for measuring the size of these regions.

In particular, we are able to perform a mapping between the properties of the inherent states of the randomly pinned system at high parental temperatures, i.e., $(T^* = \infty, p)$, with the inherent structures of the same system at low temperatures without frozen particles, i.e., $(T^*, p = 0)$. Defining $s(T^*) \equiv s(T^*, p = 0)$ and $s(p) \equiv s(T^* = \infty, p)$ and looking at the solution of $s(T^*) = s(p)$, we will show that the resulting curve $p(T^*)$ provides an estimate for a correlation length ξ, being $\xi \equiv \xi_{\rm pin} = (pN/\rho)^{1/3}$. We are then able to extract the behavior of $\xi_{\rm pin}$ as a function of T^*. It turns out that $\xi_{\rm pin}$ is compatible with a power law divergence at T_d, $\xi_{\rm pin}^3 = (T^* - T_d)^{-\alpha}$ and α not far from one.

It is worth noting that pinned particles have been intensively employed for gaining insight into the structural and dynamical properties of glassy materials in both, analytical models [9–11] and numerical simulations [12–22]. Here, in parallel with the study of $D(\omega)$ as a function of T^*, we use the method of random pinning to gain insight into the T^* dependence of the growing correlation lengths in structural glasses through the low-frequency spectrum of $D(\omega)$.

Methods.—We consider a standard 50:50 binary mixture composed of $N = N_A + N_B$ spherical particles at density $\rho = N/L^3 = 1$ [23–25]. The system is enclosed in a cubic box of side L where periodic boundary conditions are considered. Particle radii are σ_A and σ_B with $\sigma_A/\sigma_B = 1.2$ and $\sigma_A + \sigma_B \equiv \sigma = 1$ [24]. Details about numerical simulations can be found in the Supplemental Material [26] which includes Refs. [27–31]. We consider hybrid Brownian and swap Monte Carlo simulations that combine the numerical integration of the equations of motion with swap Monte Carlo moves [24]. For computing dynamical properties, i.e., the dynamical temperature T_d, the four-point susceptibility $\chi_4(t)$ [32,33], and the four-point correlation $S_4(q,t)$ [32,34–36], we consider the Brownian evolution of thermodynamically stable configurations obtained through hybrid swap-Brownian dynamics for system sizes $N = 10^3, 20^3$. The minimization of the mechanical energy has been performed through the limited-memory Broyden-Fletcher-Goldfarb-Shanno algorithm [28]. We then compute the eigenvalues of the dynamical matrix, i.e., the Hessian matrix $\mathbf{M}$, and thus we obtain the spectrum of the harmonic oscillations around the inherent structure. We also considered configurations equilibrated at high temperatures, i.e., $T^* \gg T_d$, where a finite number of particles pN, with $p \in [0,1]$, are maintained frozen during the minimization (see Ref. [7] for details). The eigenfrequencies are $\omega_\kappa^2 = \lambda_\kappa$, with λ_κ the κth eigenvalue of $\mathbf{M}$. We focus our attention on the cumulative $F(\omega) = \int_0^\omega d\omega' D(\omega')$ of the density of states $D(\omega) = \mathcal{N}^{-1} \sum_\kappa \delta(\omega - \omega_\kappa)$, with $\mathcal{N}$ the number of nonzero modes. We study the localization property of the normal-mode ω through the inverse of the participation ratio $\mathcal{R}(\omega) \equiv \sum_i |\mathbf{e}_i(\omega)|^4 / (\sum_i |\mathbf{e}_i(\omega)|^2)^2$ where $\mathbf{e}_i(\omega)$ is the eigenvector of the mode ω [37]. Let $\mathbf{r} \equiv (\mathbf{r}_1, \ldots, \mathbf{r}_N)$ be a configuration of the system thermalized at temperature T^*. We indicate with $\mathbf{r}^0 \equiv (\mathbf{r}_1^0, \ldots, \mathbf{r}_N^0)$ the configuration that minimizes the mechanical energy. We also quantify the effect of the parental temperature on the inherent configuration through the distribution $P(\Delta r) = N^{-1} \sum_i \delta(\Delta r - \Delta r_i)$, with $\Delta r_i \equiv |\mathbf{r}_i - \mathbf{r}_i^0|$, i.e., the total displacement covered by the particle i for reaching the inherent configuration $\mathbf{r}^0$ starting from $\mathbf{r}$, i.e., the thermally equilibrated one. Finally, we compare the behavior of $\xi_{\rm pin}$ with the dynamical correlation length $\xi_{\rm dyn}$ that is obtained by fitting the four-point correlation function $S_4(q, \tau_4)$ to an Ornstein-Zernike expression [34]. The structural relaxation time τ_4 has been evaluated looking at the peak of the $\chi_4(t)$ susceptibility [38,39]. Details about the computation are provided in the Supplemental Material [26].

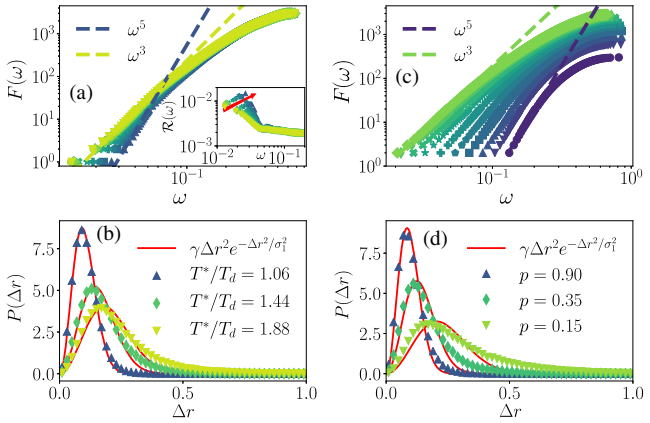

FIG. 1. (a) Cumulative density of states $F(\omega)$ as a function of the parental temperature T^* for $N = 10^3$. Temperatures decrease from yellow to blue, $T^*/T_d = 1.87, 1.56, 1.50, 1.44, 1.38, 1.31, 1.25, 1.19, 1.13, 1.06$. Inset: Inverse participation ratio $\mathcal{R}(\omega)$. (b) Probability distribution function $P(\Delta r)$ of the total displacement Δr by varying temperature. (c) Cumulative function $F(\omega)$ as the fraction of frozen particles p increases at high temperature $T^*/T_d = 3.12$. p increases from green to violet, $p = 0.05, 0.1, 0.2, 0.3, 0.4, 0.5, 0.6, 0.7, 0.8, 0.9$. (d) $P(\Delta r)$ at $T^*/T_d = 3.12$ as p increases from green to blue.

Results.—Let us start with discussing the effect of the parental temperature T^* on the cumulative function. $F(\omega)$ is shown in Fig. 1(a) for different T^* and system size $N = 10^3$. Approaching the dynamical temperature, i.e., $T^*/T_d \to 1$, the exponent of the low-frequency power law $F(\omega) \sim \omega^{s(T^*)+1}$ increases as temperature decreases, departing from the Debye value $s = 2$ to higher values. A dependency of s on both the protocol adopted for cooling down the system and T^* has been observed also in Ref. [8]. As shown in Fig. 2(a), $s + 1 \to 5$ as $T^* \to T_d$. The exponents have been computed fitting the tail of $F(\omega)$ below the boson peak [40,41] with a power law. Since the boson peak is populated by extended modes, we select the low-frequency sector through the $\mathcal{R}$ value of the mode ω.

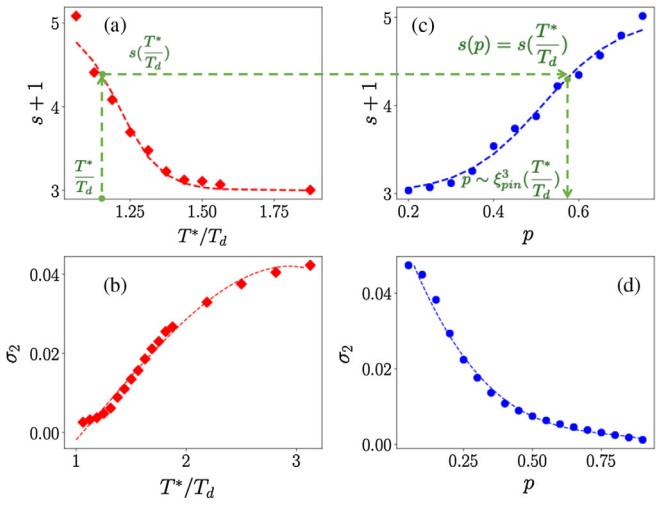

FIG. 2. (a) Slope s of the power law $F(\omega) \sim \omega^{s+1}$ as a function of the parental temperature T^* for $N = 10^3$. (b) Variance of the distribution $P(\Delta r)$ as a function of T^*. (c) Slope s as a function of p at $T^* = 3.12$. (d) Variance of the distribution $P(\Delta r)$ as a function of p at $T^* = 3.12$. Dashed lines are guides to the eye. In panels (a) and (c) the green dashed arrows sketch the mapping employed for measuring ξ_{pin}.

As one can see in the inset of Fig. 1(a), below $\omega \sim 0.04$, $\mathcal{R}$ grows as frequency decreases. Moreover, in that region, $\mathcal{R}$ grows with decreasing T^* (the arrow goes in the direction of decreasing temperatures), indicating that low-frequency modes become more localized as temperature decreases. The situation is different above $\omega \sim 0.04$ where $\mathcal{R}$ approaches the $1/N$ limit. The increasing in $\mathcal{R}(\omega)$ and the behavior $F(\omega) \sim \omega^{1+s(T^*)}$ on lowering frequency is consistent with the presence of soft-localized modes.

In order to gain insight into the nature of the rearrangements made by the system for reaching the inherent configuration $\mathbf{r}^0$, we have then computed the distribution $P(\Delta r)$ that is shown in Fig. 1(b). The distribution becomes peaked at lower and lower Δr values as temperature decreases, indicating that particles in configurations at lower temperature turn to be more caged during minimization. The red curves in Fig. 1(b) are fits to $\gamma \Delta r^2 e^{-\Delta r^2/\sigma_1^2}$, with γ and σ_1 adjustable parameters. One can notice the presence of non-Gaussian tails at high temperatures that progressively disappear for $T^* \to T_d$. The non-Gaussian tails indicate that particles travel long distances for reaching the optimal configuration when the parental configuration is taken at high T^*. As T^* decreases towards T_d, particles turn to be more caged by their neighbors and they thus perform small uncorrelated displacements to find the closer inherent structure. To be more quantitative, we have also computed the true variance σ_2 of the distribution $P(\Delta r)$, $\sigma_2(T^*)$ [see Figs. 2(b), 2(d)].

A similar phenomenology is observed looking at the system at high T^* but including a fraction of frozen particle during the research of the inherent structure [7]. In particular, when the concentration of frozen particles is large enough, moving particles are caged by the nonmoving ones. In Fig. 1(c) the cumulative $F(\omega)$ is shown at $T^*/T_d = 3.12$ by varying the fraction of frozen particles p, that increases from left to right. We have thus computed the distributions $P(\Delta r)$ when a fraction p of particles is maintained frozen and the results are shown in Fig. 1(d). Again, the red curves are the Gaussian fit. The behavior of $P(\Delta r)$ with increasing the fraction of frozen particles p is qualitatively the same obtained with decreasing temperature in the unpinned system. This is a strong indication that the same crossover from a spectrum dominated by soft-extended modes to soft-localized modes takes place in both protocols, i.e., decreasing parental temperature or increasing the fraction of pinned particles. The advantage of introducing randomly frozen particles lies in the fact that controlling p we are also controlling the typical size ξ_{pin} of frozen regions. In order to define ξ, we notice that the number of frozen particles $N_p = pN$ is naturally proportional to the volume of frozen particles V_p, thus $\xi^3 \propto pN$.

In order to make quantitative progresses, we look at the curves $s(T^*)$ and $s(p)$ obtained from $F(\omega)$, as well as at $\sigma_1(T^*)$ and $\sigma_1(p)$ [or, equivalently, at $\sigma_2(T^*)$ and $\sigma_2(p)$] obtained from $P(\Delta r)$. As already noticed $s(T^*)$ increases with decreasing T^*: this behavior is reported in Fig. 2(a). The dashed-red line is a fit to logistic curve. Similarly, the behavior of $\sigma_2(T^*)$ as a function of T^* is reported in Fig. 2(b). In panels (c) and (d) of the same figure we show the same observables as a function of the fraction of frozen particles p for configurations thermalized well above the dynamical temperature, i.e., $T^*/T_d = 3.12$.

We can thus provide a quantitative estimate of the behavior of ξ_{pin} as a function of T^* mapping the properties of the pinned system into the properties of the thermal system. In particular, we assume that, in a system where a fraction p of particles are frozen randomly in space, one introduces a correlation length $\xi_{\text{pin}} \equiv (pN/\rho)^{1/3}$. For inferring the correlation length ξ_{pin} in the real system, i.e., without artificially frozen particles, we invert the relation $\mathcal{O}(T^*, p = 0) = \mathcal{O}(T^* \gg T_d, p)$, where $\mathcal{O}$ is a generic observable, and thus we obtain a function $p(T^*)$ that allows us to measure $\xi^3_{\text{pin}}(T^*)$. The green dashed arrows in Figs. 2(a) and 2(c) give a pictorial representation of the mapping we employ to infer ξ_{pin} choosing as an observable the exponent s. The results of our analysis are shown in Fig. 3(a) for system sizes $N = 10^3, 12^3$. Diamonds are obtained considering the exponents of the power laws $s(T^*)$ and $s(p)$ as observable $\mathcal{O}$ for mapping, i.e., $\mathcal{O} \equiv s$. Circles refer to the true variance of the distribution $P(\Delta r)$, $\mathcal{O} \equiv \sigma_2$. Triangles are obtained considering the parameter σ_1 from the fit of $P(\Delta r)$ to a Gaussian distribution ($\mathcal{O} \equiv \sigma_1$). The dashed curves are the power law $\xi^3_{\text{pin}} \sim (T^* - T_d)^{-\alpha}$. The exponent α has been computed considering $\mathcal{O} = s$ and dataset $N = 10^3$

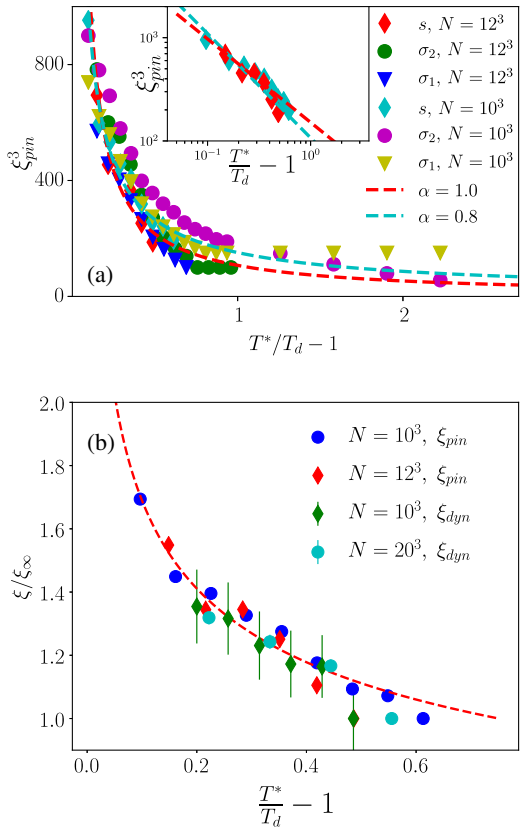

FIG. 3. (a) Correlation length $\xi^3_{\rm pin}$ defined in the main text as a function of temperature T^* and estimated through different observables for $N = 10^3, 12^3$. Diamonds refer to the $s(T^*) = s(p)$ method, circles to $\sigma_2(T^*) = \sigma_2(p)$, and triangles using σ_1, i.e., fitting $P(\Delta r)$ to $\gamma \Delta r^2 e^{-\Delta r^2/\sigma_1^2}$ and thus considering $\sigma_1(T^*) = \sigma_1(p)$. The inset highlights the behavior of $\xi^3_{\rm pin}$ computed through the exponent s for $N = 10^3, 12^3$, cyan and red symbols, respectively. Dashed lines are fits to the power law $(T^* - T_d)^{-\alpha}$ with $\alpha = 0.8$ (red) and $\alpha = 1.0$ (cyan). (b) Comparison between the correlation length $\xi_{\rm pin}$ and the dynamic length $\xi_{\rm dyn}$. ξ_∞ indicates the value of ξ at high temperatures. The red-dashed line is the best fit $(T^* - T_d)^{-\alpha/3}$ with $\alpha \sim 0.8$.

(cyan symbols), $N = 12^3$ (red symbols). We then obtain $\alpha_{\rm max} = 1.0$ and $\alpha_{\rm min} = 0.8$ for $N = 12^3, 10^3$, respectively, indicating that the exponent α varies in the range $\alpha \in [0.8, 1.0]$. As one can appreciate, different observables $\mathcal{O}$ provide estimates for ξ that are consistent with the same mild power-law divergence as T^* decreases towards T_d.

Dynamical heterogeneities are fingerprint patterns of glassy dynamics [42]. They suggest the existence of a dynamical correlation length $\xi_{\rm dyn}$ that can be estimated through multipoint correlation functions [33,35,36,38,39,43,44]. We thus compute $\xi_{\rm dyn}$ for system sizes $N = 10^3, 20^3$ and compare it with $\xi_{\rm pin}$ computed before. The result is shown in Fig. 3(b), the green circles are $\xi_{\rm dyn}$ for $N = 10^3$, cyan circles refer to $N = 20^3$. $\xi_{\rm dyn}$ has been normalized with the value of ξ at high temperature, i.e., $\xi_\infty \equiv \xi(T^* \gg T_d)$. As one can appreciate, both the correlation length $\xi_{\rm pin}$ and $\xi_{\rm dyn}$ show a mild growth that is compatible with $(T^* - T_d)^{-1/3}$.

Discussion.—In this Letter, we have explored the properties of the low-frequency excitations in a three-dimensional model glass obtained by fast quench from a well-equilibrated supercooled liquid configuration at $T = T^*$. The values of T^* spanned from high temperatures down to the dynamical transition temperature T_d. We have shown that quasilocalized soft modes progressively populate the low-frequency spectrum. The density of states of these glassy modes follows a scaling law $\omega^{s(T^*)}$ with $2 \le s(T^*) \le 4$. Far away from the dynamical transition, the low-frequency spectrum below the boson peak is well described by Debye's law, i.e., $s(T^*) = 2$. As T^* decreases, $D(\omega)$ at small ω is still power law with an exponent that is temperature dependent and deviates from Debye's law. In particular, s starts to increase its value and $s(T^*) \to 4$ for $T^* \to T_d$. As shown here and also before in Ref. [7], the same quasilogistic growth of s is observed when, instead of varying the parental temperature, we introduce a fraction p of frozen particles. Moreover, the spectrum of the low-energy excitations below the boson peak remains gapless and progressively deviates from Debye's law following a scaling $\omega^{s(p)}$, with $2 \le s(p) \le 4$. In this case, $s(p)$ increases as p increases and $s \to 4$ above a threshold value $p_{\rm th} \sim 0.5$.

The emerging phenomenology is consistent with a picture of heterogeneous regions where particles experienced different mobilities [34,42,45]. Considering a three dimensional system, an estimate of the typical linear size ξ of these heterogeneous regions in the pinned system is provided by $p^{1/3}$. This argument for the scaling of ξ together with our estimate of $p(T)$ leads to an estimate of $\xi(T)$ that is compatible with the inhomogeneous mode-coupling theory discussed in Ref. [43] where $\xi_{\rm dyn} \sim (T - T_d)^{-\nu}$ with $\nu = 1/4$.

It has been shown in Refs. [46,47] that the statistical properties of the lowest eigenfrequency of $D(\omega)$ can be employed to define a static length scale whose behavior is consistent with the point-to-set length [13,39,44,48]. Our study shows that low-frequency modes in $D(\omega)$ not only regulate the growing of a static length, and thus the changing in the thermodynamic properties of the system, but also the growing of dynamic heterogeneous patterns.

In conclusion, we showed that $D(\omega)$ provides useful information about both the structural properties of the glassy state through its inherent structures, and the dynamical properties of the corresponding supercooled equilibrium configurations at T^*. As a consequence, from $D(\omega)$ we can extract important information about the correlation length of the heterogeneous regions in supercooled liquids, which, most likely, are the ultimate origin of the instability giving rise to the non-Goldstone modes [49–55]. A recent experiment showed that $D(\omega)$ results to be modified by

natural hyperaging [56]. As a future direction, it would be interesting to investigate numerically $D(\omega)$ in the aging regime for understanding the relation between the non-Debye spectrum and aging in glasses.

G. P. acknowledges the financial support of the Simons Foundation (Grant No. 454949). G. P. and M. P. were also supported by ADINMAT, WIS-Sapienza.

*Matteo.Paoluzzi@roma1.infn.it

[1] C. Kittel, *Introduction to Solid State Physics* (Wiley, New York, 2005).
[2] R. C. Zeller and R. O. Pohl, Phys. Rev. B **4**, 2029 (1971).
[3] V. Gurarie and J. T. Chalker, Phys. Rev. B **68**, 134207 (2003).
[4] M. Baity-Jesi, V. Martín-Mayor, G. Parisi, and S. Perez-Gaviro, Phys. Rev. Lett. **115**, 267205 (2015).
[5] E. Lerner, G. Düring, and E. Bouchbinder, Phys. Rev. Lett. **117**, 035501 (2016).
[6] H. Mizuno, H. Shiba, and A. Ikeda, Proc. Natl. Acad. Sci. U.S.A. **114**, E9767 (2017).
[7] L. Angelani, M. Paoluzzi, G. Parisi, and G. Ruocco, Proc. Natl. Acad. Sci. U.S.A. **115**, 8700 (2018).
[8] E. Lerner and E. Bouchbinder, Phys. Rev. E **96**, 020104(R) (2017).
[9] C. Cammarota and G. Biroli, Proc. Natl. Acad. Sci. U.S.A. **109**, 8850 (2012).
[10] S. Franz, Europhys. Lett. **73**, 492 (2006).
[11] G. Szamel and E. Flenner, Europhys. Lett. **101**, 66005 (2013).
[12] P. Scheidler, W. Kob, K. Binder, and G. Parisi, Philos. Mag. B **82**, 283 (2002).
[13] G. Biroli, J.-P. Bouchaud, A. Cavagna, T. S. Grigera, and P. Verrocchio, Nat. Phys. **4**, 771 (2008).
[14] M. Ozawa, W. Kob, A. Ikeda, and K. Miyazaki, Proc. Natl. Acad. Sci. U.S.A. **112**, 6914 (2015).
[15] W. Kob, S. Roldán-Vargas, and L. Berthier, Nat. Phys. **8**, 164 (2012).
[16] C. Brito, G. Parisi, and F. Zamponi, Soft Matter **9**, 8540 (2013).
[17] K. H. Nagamanasa, S. Gokhale, A. Sood, and R. Ganapathy, Nat. Phys. **11**, 403 (2015).
[18] S. Karmakar and G. Parisi, Proc. Natl. Acad. Sci. U.S.A. **110**, 2752 (2013).
[19] S. Chakrabarty, S. Karmakar, and C. Dasgupta, Sci. Rep. **5**, 12577 (2015).
[20] W. Kob and D. Coslovich, Phys. Rev. E **90**, 052305 (2014).
[21] W. Kob and L. Berthier, Phys. Rev. Lett. **110**, 245702 (2013).
[22] K. Kim, Europhys. Lett. **61**, 790 (2003).
[23] B. Bernu, J. P. Hansen, Y. Hiwatari, and G. Pastore, Phys. Rev. A **36**, 4891 (1987).
[24] T. S. Grigera and G. Parisi, Phys. Rev. E **63**, 045102(R) (2001).
[25] A. Ninarello, L. Berthier, and D. Coslovich, Phys. Rev. X **7**, 021039 (2017).
[26] See Supplemental Material at http://link.aps.org/supplemental/10.1103/PhysRevLett.123.155502 for details on numerical simulations and data analysis.
[27] C. Bennemann, C. Donati, J. Baschnagel, and S. C. Glotzer, Nature (London) **399**, 246 (1999).
[28] J.-F. Bonnans, J. C. Gilbert, C. Lemaréchal, and C. A. Sagastizábal, *Numerical Optimization: Theoretical and Practical Aspects* (Springer-Verlag, Berlin, Heidelberg, New York, 2006).
[29] W. Götze, *Complex Dynamics of Glass-Forming Liquids: A Mode-Coupling Theory* (OUP, Oxford, 2008), Vol. 143.
[30] R. Yamamoto and A. Onuki, Phys. Rev. Lett. **81**, 4915 (1998).
[31] M. Paoluzzi and L. Angelani, arXiv:1905.13643.
[32] N. Laevi, F. W. Starr, T. B. Schrder, and S. C. Glotzer, J. Chem. Phys. **119**, 7372 (2003).
[33] G. Biroli and J.-P. Bouchaud, Europhys. Lett. **67**, 21 (2004).
[34] W. Kob, C. Donati, S. J. Plimpton, P. H. Poole, and S. C. Glotzer, Phys. Rev. Lett. **79**, 2827 (1997).
[35] E. Flenner, H. Staley, and G. Szamel, Phys. Rev. Lett. **112**, 097801 (2014).
[36] E. Flenner and G. Szamel, Nat. Commun. **6**, 7392 (2015).
[37] R. Bell and P. Dean, Discuss. Faraday Soc. **50**, 55 (1970).
[38] N. Laćević, F. W. Starr, T. Schrøder, and S. Glotzer, J. Chem. Phys. **119**, 7372 (2003).
[39] G. Biroli, S. Karmakar, and I. Procaccia, Phys. Rev. Lett. **111**, 165701 (2013).
[40] U. Buchenau, N. Nücker, and A. J. Dianoux, Phys. Rev. Lett. **53**, 2316 (1984).
[41] K. Binder and W. Kob, *Glassy Materials and Disordered Solids: An Introduction to Their Statistical Mechanics* (World Scientific, Singapore, 2011).
[42] L. Berthier and G. Biroli, Rev. Mod. Phys. **83**, 587 (2011).
[43] G. Biroli, J.-P. Bouchaud, K. Miyazaki, and D. R. Reichman, Phys. Rev. Lett. **97**, 195701 (2006).
[44] S. Karmakar, C. Dasgupta, and S. Sastry, Proc. Natl. Acad. Sci. U.S.A. **106**, 3675 (2009).
[45] N. Laevi, F. W. Starr, T. B. Schrder, and S. C. Glotzer, J. Chem. Phys. **119**, 7372 (2003).
[46] S. Karmakar, E. Lerner, and I. Procaccia, Physica (Amsterdam) **391A**, 1001 (2012).
[47] R. Gutiérrez, S. Karmakar, Y. G. Pollack, and I. Procaccia, Europhys. Lett. **111**, 56009 (2015).
[48] L. Berthier and W. Kob, Phys. Rev. E **85**, 011102 (2012).
[49] W. Schirmacher, Europhys. Lett. **73**, 892 (2006).
[50] W. Schirmacher, G. Ruocco, and T. Scopigno, Phys. Rev. Lett. **98**, 025501 (2007).
[51] W. Schirmacher, B. Schmid, C. Tomaras, G. Viliani, G. Baldi, G. Ruocco, and T. Scopigno, Phys. Status Solidi C **5**, 862 (2008).
[52] A. Marruzzo, S. Köhler, A. Fratalocchi, G. Ruocco, and W. Schirmacher, Eur. Phys. J. Spec. Top. **216**, 83 (2013).
[53] A. Marruzzo, W. Schirmacher, A. Fratalocchi, and G. Ruocco, Sci. Rep. **3**, 1407 (2013).
[54] C. Tomaras and W. Schirmacher, J. Phys. Condens. Matter **25**, 495402 (2013).
[55] W. Schirmacher, T. Scopigno, and G. Ruocco, J. Non-Cryst. Solids **407**, 133 (2015).
[56] E. A. A. Pogna, A. I. Chumakov, C. Ferrante, M. A. Ramos, and T. Scopigno, J. Phys. Chem. Lett. **10**, 427 (2019).